*Articles*

# Arg$^{362}$ and Tyr$^{365}$ of the Botulinum Neurotoxin Type A Light Chain Are Involved in Transition State Stabilization†

Thomas Binz,*,‡ Steffen Bade,‡ Andreas Rummel,‡ Astrid Kollewe,‡ and Jürgen Alves§

*Department of Biochemistry and Department of Biophysical Chemistry, Medizinische Hochschule Hannover, Hannover, Germany*

*Received September 25, 2001; Revised Manuscript Received December 10, 2001*

ABSTRACT: The botulinum neurotoxin type A (BoNT/A) light chain (LC) acts as zinc endopeptidase. The X-ray structure of the toxin demonstrated that $Zn^{2+}$ is coordinated by His$^{222}$ and His$^{226}$ of the $Zn^{2+}$ binding motif HisGluXXHis and Glu$^{261}$, whereas Glu$^{223}$ coordinates the water molecule required for hydrolysis as the fourth ligand. Recent analysis of a cocrystal of the BoNT/B LC and its substrate synaptobrevin 2 suggested that Arg$^{362}$ and Tyr$^{365}$ of the homologous BoNT/A may be directly involved in catalysis. Their role and that of Glu$^{350}$ which is also found in the vicinity to the active site were analyzed by site-directed mutagenesis. Various replacements of Arg$^{362}$ and substitution of Tyr$^{365}$ with Phe resulted in 79- and 34-fold lower $k_{cat}/K_m$ values, respectively. These changes were provoked by decreased catalytic rates ($k_{cat}$) and not by alterations of ground state substrate binding as evidenced by largely unchanged $K_d$ and $K_m$ values. None of these mutations affected the overall secondary structure or zinc content of the LC. These findings suggest that the guanidino group of Arg$^{362}$ and the hydroxyl group of Tyr$^{365}$ together accomplish transition state stabilization as was proposed for thermolysin, being the prototypical member of the gluzincin superfamily of metalloproteases. Mutation of Glu$^{350}$ dramatically diminished the hydrolytic activity which must partly be attributed to an altered active site fine structure as demonstrated by an increased sensitivity toward heat-induced denaturing and a lower $Zn^{2+}$ binding affinity. Glu$^{350}$ apparently occupies a central position in the active site and presumably positions His$^{222}$ and Arg$^{362}$.

The group of clostridial neurotoxins includes tetanus toxin (TeNT)[1] and seven botulinum neurotoxins (BoNTs, serotypes A−G). Each of these toxins consists of three functionally distinct domains. The carboxyl-terminal half of the ∼100 kDa heavy chain (HC), the $H_C$ fragment, mediates selective binding to neuronal cells via specific gangliosides. The amino-terminal half of the HC, the $H_N$ fragment, is thought to translocate the light chain (LC) into the cytosol after receptor-mediated endocytosis of the entire molecule. The ∼50 kDa LCs are zinc endopeptidases and exclusively hydrolyze members of the three SNARE (soluble NSF attachment protein receptor) families. VAMP (vesicle-associated membrane protein)/synaptobrevin represents the substrate for BoNT/B, -D, -F, and -G and TeNT, whereas BoNT/A, -C, and -E cleave SNAP-25 (25 kDa synaptosome-associated protein). Except for BoNT/B and TeNT, which share the same cleavage site, hydrolysis occurs in unique positions. BoNT/C is in addition capable of hydrolyzing syntaxin. Cleavage of any of the neuronal SNAREs results in inhibition of the fusion of synaptic vesicles with the presynaptic membrane, and thus a blockade of neurotransmitter release (*1*, *2*).

The LCs of clostridial neurotoxins constitute a new family of zinc metalloproteases (family M27; *3*, *4*) and display unique substrate specificity. Unlike most other proteases, they fail to hydrolyze short peptides comprising the individual cleavage sites and cleave only one of several identical peptide bonds present in their respective substrate molecule (*5*−*7*).

The active site residues of clostridial neurotoxin LCs responsible for $Zn^{2+}$ binding have been determined for various serotypes by site-directed mutagenesis and X-ray structure analysis. These studies unequivocally demonstrated that the two histidine residues of the $Zn^{2+}$ binding motif HisGluXXHis and another glutamic acid residue found in a separate peptide sequence approximately 35 residues downstream directly coordinate the zinc ion (*8*−*11*). A water molecule occupies the fourth position, which is held in place by the catalytic glutamate residue of the $Zn^{2+}$ binding motif. This mode of $Zn^{2+}$ coordination classifies clostridial neu-

† This work was supported by a grant from the Deutsche Forschungsgemeinschaft (IIB2-Bi 660/1-2) to T.B.

* To whom correspondence should be addressed: Department of Biochemistry, OE 4310, Medizinische Hochschule Hannover, 30625 Hannover, Germany. Phone: +49 511-532-2859. Fax: +49 511-532-2827. E-mail: binz.thomas@mh-hannover.de.

‡ Department of Biochemistry.

§ Department of Biophysical Chemistry.

[1] Abbreviations: BoNT, botulinum neurotoxin; CD, circular dichroism; HC, heavy chain; $H_C$, carboxyl-terminal fragment of the heavy chain; $H_N$, amino-terminal fragment of the heavy chain; LC, light chain; NSF, *N*-ethylmaleimide sensitive fusion protein; PCR, polymerase chain reaction; SDS−PAGE, sodium dodecyl sulfate−polyacrylamide gel electrophoresis; SNAP-25, 25 kDa synaptosome-associated protein; SNARE, soluble NSF attachment protein receptor; TeNT, tetanus neurotoxin; VAMP, vesicle-associated membrane protein.

10.1021/bi0157969 CCC: $22.00 
Published on Web 01/12/2002

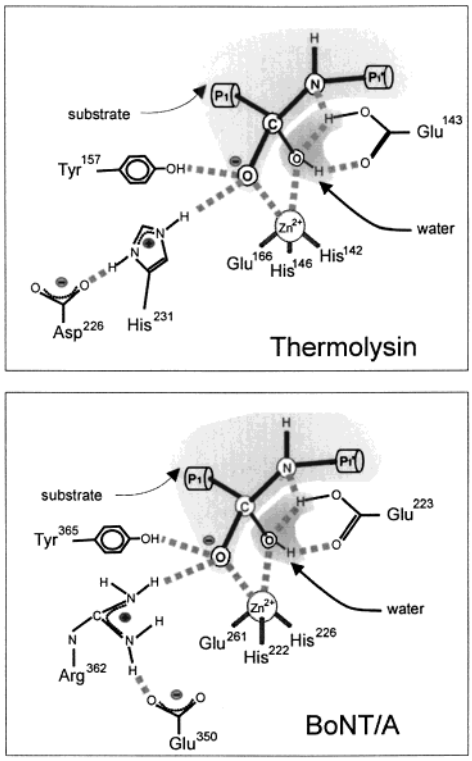


FIGURE 1: Proposed hydrolytic mechanism of thermolysin (top panel) and similarity of the arrangement of active site residues to that of LC/A. In the first step, a water molecule polarized by $Glu^{143}$ ($Glu^{223}$ in LC/A) and $Zn^{2+}$ nucleophilically attacks the carbonyl carbon of the scissile peptide bond to form an oxyanion. The amino acid side chains implicated in stabilization of the negative charges that develop in the tetrahedral transition state on the carbonyl carbon atoms are depicted. $Asp^{226}$ ($Glu^{350}$ in LC/A) is suggested to keep $His^{231}$ ($Arg^{362}$ in LC/A) in the proper position through a hydrogen bonding interaction. Peptide bond cleavage is likely achieved by a proton transfer from the attacking water mediated by the carboxyl group of $Glu^{143}$ ($Glu^{223}$ in LC/A) to form a protonated amine. The nomenclature used for substrate amino acids is that from Schechter and Berger (*29*). This figure was modified from Fernandez et al. (*28*).

rotoxin LCs as being in the gluzincin superfamily (clan MA; *4*) of metalloproteases with thermolysin being the prototypical member.

In thermolysin, catalysis follows a general base-type mechanism (*12*). In the proposed mechanism, a polarized water molecule, ligated to $Glu^{143}$ of the HisGluXXHis motif and $Zn^{2+}$, nucleophilically attacks the carbonyl carbon of the scissile peptide bond to form an oxyanion [Figure 1 (top panel)]. Simultaneously, a proton abstracted from the attacking water is shuttled via the carboxyl group of $Glu^{143}$ to the scissile peptide bond nitrogen, and $Glu^{143}$ may then stabilize the tetrahedral intermediate by a salt bridge with the positively charged amide nitrogen. The negative charge that develops on the carbonyl oxygen atom in the tetrahedral transition state is stabilized by hydrogen bonding interactions with a protonated histidine, $His^{231}$, and the hydroxyl group of $Tyr^{157}$. It is assumed that $His^{231}$ is retained in the proper position and the protonated state through a hydrogen bonding interaction with $Asp^{226}$. The protonated amide nitrogen facilitates disruption of the C−N bond and may subsequently receive a second proton derived from the water, possibly again mediated by the carboxyl group of $Glu^{143}$ (*12*).

The catalytic mechanism of clostridial neurotoxin LCs remains to be established. X-ray structure analysis of LC/B bound to its substrate VAMP/synaptobrevin 2 indicated that $Arg^{369}$ and $Tyr^{372}$ line up in the proximity of the scissile peptide bond and are strictly conserved throughout all clostridial neurotoxin LCs (*13*). Thus, an involvement of these residues in substrate binding or in the catalytic process is obvious. The importance of the tyrosine residue in substrate cleavage was very recently pointed out for the TeNT LC (*14*). Kinetic data, however, which would allow conclusions to be drawn with respect to the catalytic mechanism, are not available.

We have studied their functional significance by conducting site-directed mutagenesis of $Arg^{362}$ and $Tyr^{365}$, the corresponding amino acid residues of LC/A, and kinetic analyses of the generated mutants. Furthermore, we assessed the impact of $Glu^{350}$, another strictly conserved residue of the active site. A conservative replacement of $Tyr^{365}$ with phenylalanine was chosen to rule out potential implications on the LC's fine structure at the active center. $Arg^{362}$ and $Glu^{350}$ were substituted with lysine, histidine, or alanine and glutamine or alanine, respectively. Mutation of $Arg^{362}$ and of $Tyr^{365}$ caused a substantial reduction in $k_{cat}$ values, but did not significantly affect $Zn^{2+}$ or substrate binding. Removal of the negative charge of $Glu^{350}$ dramatically diminished the hydrolytic activity, which must, however, partly be ascribed to a lower $Zn^{2+}$ binding affinity and alterations of the fine structure at the active site.

## MATERIALS AND METHODS

*Molecular Modeling.* Molecular modeling was carried out using an octane workstation (Silicon Graphics Inc., Mountain View, CA) and Insight II 2000 software (Molecular Simulations Inc., San Diego, CA).

*Plasmid Constructions.* pSNAP-25His6 was generated by subcloning the *Eco*RI−*Sal*I fragment of the equivalent pQE3 (Qiagen, Hilden, Germany) expression plasmid, pBN10 (*15*), in pSP73 (Promega, Mannheim, Germany) cleaved correspondingly. pGEX-SNAP-25($Arg^{198}$Glu) was constructed by employing the backward primer 5′-TCTCGAATTCTTATCCCAGCATCTTTGTTGCTTCTTGGTTGGCTTCATC-3′ for PCR and the *Bam*HI and *Eco*RI sites of pGEX-2T (Amersham Pharmacia Biotech, Freiburg, Germany). Mutants of LC/A-$Arg^{362}$ and -$Tyr^{365}$ were generated by PCR using pBN3, encoding wild-type LC/A (*16*), as template DNA and the forward primers 5′-TCTCAGTACTTAACGCGAAAACATATTTGAATTTTGATAAAG-3′ ($Arg^{362}$Ala), 5′-TCTCAGTACTTAACCACAAAACATATTTGAATTTTGATAAAG-3′ ($Arg^{362}$His), 5′-TCTCAGTACTTAACAAGAAAACATATTTGAATTTTGATAAAG-3′ ($Arg^{362}$Lys), and 5′-TCTCAGTACTTAACAGAAAAACATTTTTGAATTTTGATAAAGCCGT-3′ ($Tyr^{365}$Phe). The PCR fragments were cut with *Sca*I and *Pst*I and inserted into pBN3, cleaved correspondingly. Mutants of LC/A-$Glu^{350}$ were created using the oligonucleotides 5′-TCTCTAGATCTACACAGCTGATAATTTTGTTAAGTTTTTT-3′ ($Glu^{350}$Ala) and 5′-TCTCTAGATCTACACACAGGATAATTTTGTTAAGTTTTTT-3′ ($Glu^{350}$Gln). The PCR fragments were cleaved with *Bgl*II and *Pst*I and ligated together with a *Bsp*68I−*Bgl*II fragment generated by PCR employing the backward primer 5′-CTGTGTAGATCTCTGTTAACATT-

TTG-3′ into pBN3 cut with *Bsp*68I and *Pst*I. Nucleotide sequences of all mutants were verified by DNA sequencing.

*Purification of Recombinant Proteins.* Recombinant LC/A and its mutants were expressed utilizing *Escherichia coli* strain M15pREP4 (Qiagen) during 3 h of incubation at 21 °C and purified on Ni−nitrilotriacetic acid−agarose beads (Qiagen) according to the manufacturer's instructions. Fractions containing the LCs were dialyzed against toxin assay buffer [150 mM potassium glutamate and 10 mM HEPES-KOH (pH 7.2)] or 20 mM Tris (pH 7.2) containing 100 mM NaCl for spectroscopic analyses, frozen in liquid nitrogen, and kept at −70 °C.

GST and GST−SNAP-25(Arg$^{198}$Glu) were affinity purified on glutathione (GT) Sepharose (Amersham Pharmacia Biotech) according to the method of Guan and Dixon (*17*) and finally dialyzed against toxin assay buffer.

*In Vitro Transcription and Translation.* SNAP-25His$_6$ was synthesized in vitro from the plasmid pSNAP-25His6 using the TNT-coupled reticulocyte lysate system (Promega) in the presence of [$^{35}$S]methionine (555 KBq, >37 TBq/mmol; Amersham Pharmacia Biotech) in a total volume of 25 $\mu$L.

*Endopeptidase Assay.* In standard assays, 5 $\mu$M SNAP-25His$_6$ was incubated in the presence of a final concentration of wild-type LC/A or its mutants of 2 nM in a total volume of 100 $\mu$L in toxin assay buffer at 37 °C. Aliquots (15 $\mu$L) were withdrawn at specified time intervals. Reactions were stopped by mixing with 15 $\mu$L of ice-cold double-concentrated sample buffer [120 mM Tris-HCl (pH 6.75), 10% (v/v) $\beta$-mercaptoethanol, 4% (w/v) SDS, 20% (w/v) glycerol, and 0.014% (w/v) bromophenol blue]. Samples were boiled for 3 min and subjected to SDS−PAGE on 12.5% gels at a constant current of 20 mA. Proteins were visualized by staining with Coomassie Blue and quantified with a Sharp JX-325 high-resolution scanner employing an ImageMaster TM 1-D program (version 1.10; Amersham Pharmacia Biotech).

For the determination of the enzyme kinetic parameters, the substrate concentration was set to 3.0, 4.5, 6.8, 10.1, or 15.2 $\mu$M using recombinant SNAP-25His$_6$. Each of the various substrate concentrations was endowed by the addition of 1 $\mu$L of radiolabeled SNAP-25His$_6$. Incubation was carried out in a final volume of 40 $\mu$L of toxin assay buffer. After incubation for 2 or 4 min at 37 °C, aliquots (18 $\mu$L) were taken and the enzymatic reaction was stopped by mixing with 9 $\mu$L of prechilled 3-fold concentrated SDS−PAGE sample buffer. SNAP-25 and its cleavage products were separated by SDS−PAGE, and the radiolabeled protein was visualized using a BAS-1500 phosphor imager (Fuji Photo Film). The percentage of hydrolyzed SNAP-25 was determined from the turnover of the radiolabeled substrate by applying the Tina 2.09f program (Raytest Isotopenmessgeräte GmbH, Straubenhardt, Germany) and used to calculate the initial velocity of substrate hydrolysis. Previous experiments had demonstrated that the kinetics of hydrolysis of radiolabeled SNAP-25His$_6$ are indistinguishable from those of recombinant SNAP-25His$_6$ (data not shown). $K_m$ and $V_{max}$ values were derived from Lineweaver−Burk plots using the GraphPad Prism 1.00 program (GraphPad Software Inc.).

*Binding Assay.* The LC/A insensitive fusion protein GST−SNAP-25(Arg$^{198}$Glu) (0.05−0.25 nmol) prebound to 10 $\mu$L of GT Sepharose beads was suspended in 190 $\mu$L of toxin assay buffer containing 0.02% Triton X-100. Beads were then incubated for 2 h at 4 °C in the presence of various concentrations of wild-type LC/A or its mutants ranging from 156 to 2500 nM. The beads were collected by centrifugation. Unbound material in the supernatant fraction was transferred into a new tube. The pellet fraction was washed three times each with 40 bed volumes of toxin assay buffer. The washed pellet fraction was boiled in SDS sample buffer and analyzed together with the supernatant fraction by SDS−PAGE as described above. The amount of bound LC was quantified by densitometric scanning following Coomassie Blue staining and corrected for nonspecific binding by subtracting the value obtained for binding to GST. $K_d$ values for LC binding to SNAP-25(Arg$^{198}$Glu) were calculated by Scatchard plot analysis using the program GraphPad Prism 1.00.

*Circular Dichroism Spectroscopy.* CD data were collected with a Dichrograph III (Jobin-Yvon) spectropolarimeter equipped with a computer-controlled temperature cuvette holder. Far-UV data in the range of 200−250 nm were obtained with a 0.1 mm path length cuvette containing 0.5−0.8 mg/mL protein in 20 mM Tris buffer (pH 7.2) supplemented with 100 mM NaCl. CD spectra were recorded at room temperature (21 °C) at a speed of 6 nm/min with a response time of 2 s. Secondary structure content was calculated using the CDPro software by Sreerama and Woody (*18*).

Temperature-induced denaturation was conducted in 50 mM sodium phosphate buffer (pH 7.5) supplemented with 100 mM NaCl at a protein concentration of 50 $\mu$g/mL by monitoring the CD signal at 220 nm in a 0.4 cm path length cuvette. The temperature increase per time of 0.9 °C/min from 25 to 80 °C was measured directly in the protein solution with a thermistor.

*Zinc Content Determination.* LC/A preparations designated for zinc content determinations were extensively dialyzed against 20 mM Tris buffer (pH 7.2) containing 100 mM NaCl. Absorbance peaks were measured in duplicates at 213.9 nm using a Zeiss AAS5 FL atomic absorption spectrometer. Zinc concentrations in the LC samples (0.5 mg/mL) were corrected for residual zinc in the buffer.

## RESULTS

*Enzymatic Activity of Various LC/A Active Site Mutants.* Replacement of Tyr$^{365}$ and Arg$^{362}$ with phenylalanine and alanine, respectively, drastically diminished the hydrolytic activity of LC/A as shown in Figure 2. The double mutant Arg$^{362}$Ala/Tyr$^{365}$Phe proved to be completely inactive even when tested at a final concentration of 3 $\mu$M (data not shown). Since the corresponding amino acid of Arg$^{362}$ in the active center of thermolysin is a histidine, we assessed whether the positively charged side groups of histidine or lysine would restore full enzyme activity. However, both residues could not substitute the guanidino group of the genuine arginine residue. Interestingly, under the applied experimental conditions, mutants of Glu$^{350}$ exhibited no hydrolytic activity. Substrate hydrolysis could only be detected at LC concentrations exceeding 100 nM, reaching 6% cleavage within 1 h of incubation at 37 °C (data not shown).

*Kinetic Parameters of SNAP-25 Hydrolysis.* Analysis of enzyme kinetics was performed by determining the initial cleavage rate of recombinant SNAP-25 at varying concentra-

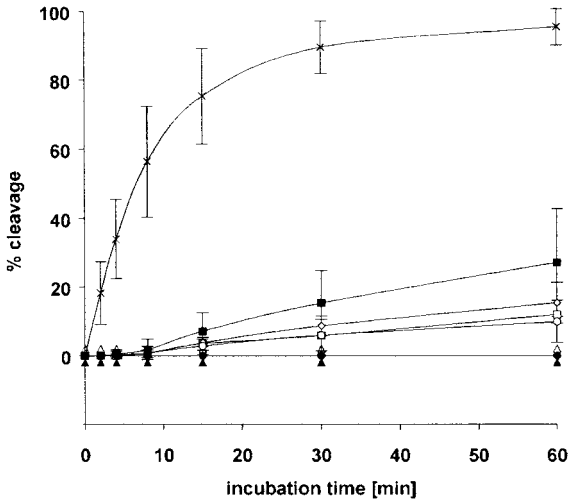


FIGURE 2: Hydrolytic activity of LC/A and of various mutants. The cleavage rates were determined at 37 °C in a total volume of 100 $\mu$L of toxin assay buffer using 5 $\mu$M SNAP-25His$_6$ and a final concentration of LCs of 2 nM. Aliquots of the reaction mixtures were taken at the time points indicated and analyzed by 12.5% SDS−PAGE and Coomassie Blue staining. Amounts of proteins were quantified by densitometric scanning. Data represent means ± standard deviation of three to nine independent experiments: wild-type LC/A (×), LC/A(Tyr$^{365}$Phe) (■), LC/A(Arg$^{362}$Lys) (□), LC/A(Arg$^{362}$His) (◇), LC/A(Arg$^{362}$Ala) (○), LC/A(Glu$^{350}$Ala) (▲), LC/A(Glu$^{350}$Gln) (△), and LC/A(Arg$^{362}$Ala/Tyr$^{365}$Phe) (●).

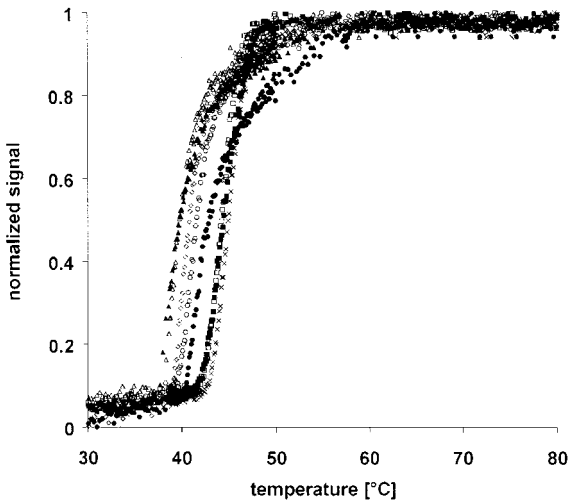


FIGURE 3: Temperature-induced denaturing of wild-type LC/A and various mutants. The CD signal at 220 nm was monitored in 50 mM sodium phosphate buffer (pH 7.5) supplemented with 100 mM NaCl by applying LC concentrations of 50 $\mu$g/mL and a temperature increase of 0.9 °C/min from 25 to 80 °C: wild-type LC/A (×), LC/A(Tyr$^{365}$Phe) (■), LC/A(Arg$^{362}$Lys) (□), LC/A(Arg$^{362}$His) (◇), LC/A(Arg$^{362}$Ala) (○), LC/A(Glu$^{350}$Ala) (▲), LC/A(Glu$^{350}$Gln) (△), and LC/A(Arg$^{362}$Ala/Tyr$^{365}$Phe) (●).

Table 1: Enzyme Kinetic Parameters of Wild-Type LC/A and Various Mutants[a]

| LC | $K_m$ ($\mu$M) | $k_{cat}$ (min$^{-1}$) | $k_{cat}/K_m$ ($\mu$M$^{-1}$ min$^{-1}$) |
|---|---|---|---|
| wild-type | 9.8 ± 3.1 | 1026 ± 424 | 113 |
| Arg$^{362}$Ala | 7.9 ± 1.9 | 12.2 ± 2.0 | 1.65 |
| Arg$^{362}$Lys | 9.6 ± 1.5 | 16.9 ± 5.1 | 1.82 |
| Arg$^{362}$His | 16.1 ± 4.2 | 11.5 ± 4.1 | 0.82 |
| Tyr$^{365}$Phe | 9.5 ± 2.8 | 29.0 ± 9.5 | 3.36 |
| Arg$^{362}$Ala/Tyr$^{365}$Phe | | not detectable | |
| Glu$^{350}$Ala | 12.3 ± 3.0 | 0.16 ± 0.03 | 0.013 |
| Glu$^{350}$Gln | 9.3 ± 2.6 | 0.10 ± 0.03 | 0.011 |

[a] Values represent means ± standard deviation from three to eleven independent measurements.

tions. Lineweaver−Burk plots were created, and $K_m$ and $k_{cat}$ values were derived from the *X*- and *Y*-intercepts, respectively. The results are presented in Table 1. The calculated $k_{cat}/K_m$ value for wild-type LC/A of 113 $\mu$M$^{-1}$ min$^{-1}$ was considerably higher than the value of 3.2 $\mu$M$^{-1}$ min$^{-1}$ from an earlier study (*19*). In contrast to this work, we used a HEPES-based buffer devoid of $Na^+$ and $Cl^-$ ions. In the case of BoNT/B, HEPES proved to be the optimal compound of the buffer substances that were tested, and NaCl was shown to hamper the endopeptidase activity of that enzyme (*20*). Therefore, the increased hydrolytic activity of LC/A may primarily be attributed to the altered buffer solution.

Removal of the hydroxyl group of LC/A-Tyr$^{365}$ caused a 34-fold decrease in $k_{cat}$ compared to that of wild-type LC/A, whereas no significant change in the $K_m$ value was observed. Exchange of Arg$^{362}$ with alanine (a deletion of the positive charge) also resulted in drastic decline in the $k_{cat}$ value with no significant alteration of $K_m$. Substitution of Arg$^{362}$ with amino acids carrying positively charged side chains, i.e., histidine, the proposed counterpart in thermolysin, and lysine, displayed ~80-fold lower $k_{cat}$ values [like LC/A(Arg$^{362}$Ala)]. The mutation to lysine did not affect $K_m$, while introduction of histidine slightly increased $K_m$. The kinetic constants determined for LC/A(Glu$^{350}$Ala) and -(Glu$^{350}$Gln) should be interpreted with care, since appropriate experiments, i.e., cleavage under substrate saturation conditions, could not be conducted due to the extremely low hydrolytic activity.

*Spectroscopic Structure Analyses.* To exclude the possibility that the individual mutations had affected structural elements of the LC, far-UV CD spectra were recorded. The spectra of all mutants were essentially indistinguishable from the wild-type trace (data not shown). The mean values of their secondary structure contents were 37 ± 4% α-helix, 16 ± 1% $\beta$-strand, 17 ± 2% turn, and 30 ± 2% random coil.

In a further attempt to probe the conformation of the mutated LCs, temperature-induced denaturing measurements were conducted. Changes in the molar ellipticity at 220 nm were recorded as a function of temperature (Figure 3). The unfolding charts are well described by steeply sigmoidal curves with the melting temperatures ($T_m$) being given by their inflection points. The traces obtained for wild-type LC/A, LC/A(Arg$^{362}$Lys), and LC/A(Tyr$^{365}$Phe) were virtually identical, yielding $T_m$ values of 44.8, 44.4, and 43.5 °C, respectively, that were within the inaccuracy of ~0.7 °C for measurements of the same sample. LC/A(Arg$^{362}$Ala), -(Arg$^{362}$His), -(Glu$^{350}$Gln), and -(Glu$^{350}$Ala), however, exhibited slightly lower $T_m$ values of 38.4−40.2 °C. It should be noticed, that the unfolding process started only at temperatures above 38 °C, denoting that all mutants were unharmed under the conditions used for the proteolysis assays. The lower thermostability of mutants of Glu$^{350}$ could be explained by the loss of the ionic interaction between Arg$^{362}$ and Glu$^{350}$, which may promote the occurrence of alternate conformations around the active site that are more sensitive to unfolding at elevated temperatures. With regard to LC/A(Arg$^{362}$His), the two energetically most favored rotamers of the histidine side group bend away from Glu$^{350}$ and presumably step into a $\pi$-stacking interaction with the

Table 2: Substrate Binding of Wild-Type LC/A and Various Mutants[a]

| LC | $K_d$ ($\mu$M) | LC | $K_d$ ($\mu$M) |
|---|---|---|---|
| wild-type | 0.233 ± 0.031 | $Tyr^{365}Phe$ | 0.240 ± 0.066 |
| $Arg^{362}Ala$ | 0.244 ± 0.046 | $Arg^{362}Ala/Tyr^{365}Phe$ | 0.247 ± 0.052 |
| $Arg^{362}Lys$ | 0.234 ± 0.029 | $Glu^{350}Ala$ | 0.295 ± 0.097 |
| $Arg^{362}His$ | 0.299 ± 0.052 | $Glu^{350}Gln$ | 0.371 ± 0.088 |

[a] Values represent means ± standard deviation from three to five independent measurements.

Table 3: Zinc Content of Wild-Type LC/A and Various Mutants[a]

| LC | $Zn^{2+}$ (mol/mol of protein) |
|---|---|
| wild-type | 0.71 ± 0.13 |
| $Arg^{362}Ala$ | 0.59 ± 0.13 |
| $Arg^{362}Lys$ | 0.78 ± 0.24 |
| $Arg^{362}His$ | 0.67 ± 0.22 |
| $Tyr^{365}Phe$ | 0.68 ± 0.18 |
| $Arg^{362}Ala/Tyr^{365}Phe$ | 0.79 ± 0.09 |
| $Glu^{350}Ala$ | 0.50 ± 0.12 |
| $Glu^{350}Gln$ | 0.44 ± 0.17 |

[a] Values represent means ± standard deviation from three independent measurements.

phenyl ring of $Phe^{195}$. In addition, H-bond interactions of the imidazole NH group with the $Asp^{369}$ carboxylate or the carbonyl oxygen of the $Asn^{367}$ backbone are likely to build. Together, these interactions could locally deform the structure of the LC substrate binding cavity and thus provide a plausible explanation for the reduced stability and the above-described slight increase in $K_m$.

*Substrate Binding Analysis.* Substrate binding of the various LC mutants was examined by employing SNAP-25($Arg^{198}Glu$). Earlier studies proved that this mutant resists cleavage by LC/A in vitro (*16*). Consequently, we could study binding in the absence of substrate hydrolysis. The amount of bound LC was plotted versus the ratio of bound to free LC according to Scatchard analysis, and $K_d$ values were derived from the slope of the resulting regression lines. The obtained results are summarized in Table 2. The binding affinity of 0.23 $\mu$M determined for wild-type LC/A was somewhat lower compared to earlier findings (0.19 $\mu$M; *16*). As in these experiments wild-type SNAP-25 and hydrolytically inactive LC/A($Glu^{223}Gln$) were used, this discrepancy may indicate that the arginine to glutamate exchange in the substrate P1′ position interferes to a minor extent with the stability of the enzyme−substrate complex. Importantly, the $Tyr^{365}$ to phenylalanine and $Arg^{362}$ to alanine or lysine mutations did not effect the interaction of LC/A with SNAP-25. Mutation of $Glu^{350}$ and the exchange of $Arg^{362}$ with histidine caused slightly higher $K_d$ values.

*Zinc Content Determination.* To probe the configuration of amino acids at the LC active center, the zinc content was measured by atomic absorption spectroscopy. As depicted in Table 3, the amount of bound zinc per mole of recombinant wild-type LC/A was somewhat <1. This observation represents a common finding with purified clostridial neurotoxins and other metalloproteases (*21*) and also agrees with recently obtained results for the recombinant TeNT LC (*14*). Importantly, mutation of $Arg^{362}$ and of $Tyr^{365}$ as well as a joint mutation of both residues did not provoke a reduction in the amount of bound zinc, indicating an intact fine structure around the active site. In contrast, replacement of $Glu^{350}$ with glutamine or alanine generated LCs with slightly lower zinc content than the wild-type protease.

## DISCUSSION

Recent crystallographic analyses of BoNT/A and BoNT/B revealed, besides the residues coordinating the $Zn^{2+}$ ion in a tetrahedral fashion, another glutamate, a tyrosine, and an arginine around the active site, which are strictly conserved throughout all serotypes of clostridial neurotoxins (*1*, *9*, *10*). Their structural configuration closely resembles that of the active site of other gluzincin metalloproteases (Figure 1), of which thermolysin constitutes the prototypical member. Furthermore, the tyrosine and arginine residues of BoNT/B line up in the proximity of the peptide bond to be hydrolyzed as evidenced by the X-ray structure of LC/B bound to its substrate synaptobrevin 2 (*13*). However, X-ray structures do not provide insights regarding the catalytic mechanism. A precise elucidation of the catalytic mechanism of clostridial neurotoxins is an important issue for the characterization of this new group of metalloproteases and the development of efficient inhibitors.

*Role of $Arg^{362}$ and $Tyr^{365}$ in Substrate Hydrolysis.* $Arg^{362}$ and $Tyr^{365}$ could participate in various manners in the catalytic process. First, the side chain of the tyrosine could donate a proton to the amide nitrogen of the scissile peptide bond to generate a more favorable leaving group as suggested for LC/B by Hanson and Stevens (*13*). A putative role of the arginine side group could consist of polarizing the attacking water molecule as the first step of catalysis (*22*). Alternatively, the side groups of both amino acids could be implicated in stabilizing the carbonyl oxygen atom in the transition state as reported for thermolysin-like proteases (*23*, *24*). In this study, we approached this issue. We demonstrate that mutation of $Arg^{362}$ and of $Tyr^{365}$ does not provoke any relevant structural alterations as illustrated by similar zinc contents, virtually identical far-UV CD spectra, and basically similar sensitivities toward heat-induced denaturing. Also, mutation of $Arg^{362}$ and of $Tyr^{365}$ does not significantly interfere with ground state substrate binding as evidenced by largely unaltered $K_m$ and $K_d$ values of the individual mutants. In contrast, any mutation of the two residues drastically impaired $k_{cat}$, supporting a contribution to the catalytic process.

Since mutation of $Arg^{362}$ and $Tyr^{365}$ led to enzymes displaying a readily detectable residual protease activity, our data are thus clearly in favor of a less crucial role in catalysis for both residues, such as participation in transition state binding. This idea is supported by the calculated differences in the free energy required for transition state stabilization $\{\Delta\Delta G = -RT \ln[(k_{cat}/K_m)_{mutant}/(k_{cat}/K_m)_{wild-type}]\}$ of ~10.9 and ~9.0 kJ/mol for mutants of $Arg^{362}$ and $Tyr^{365}$, respectively, which are consistent with the loss of one hydrogen bonding interaction with the oxyanion (*25*). Similarly altered $\Delta\Delta G$ values were determined for mutants of residues proposed to be involved in transition state stabilization of other metalloproteases (*24*, *26*).

The decrease in $k_{cat}/K_m$ values by factors of 34 and ~80 for mutants of $Tyr^{365}$ and $Arg^{362}$, respectively, indicates a slightly less important role of tyrosine in transition state stabilization compared to that of $Arg^{362}$. Mutational analysis of the corresponding residues of enzymes of the thermolysin

family provided a similar discrepancy between the contribution of those two residues (*23*, *24*), underscoring the closely related catalytic mechanisms of these two gluzincin families (Figure 1).

Transition state stabilization of the oxyanion appeared no longer to be attainable with conservative exchanges of $Arg^{362}$ with lysine or histidine, since the resulting difference in side chain length of ~1.6 or ~2.2 Å, respectively, affected the enzymatic activity to an extent similar to that of the mutation to alanine. Thus, the active site amino acids are apparently rigidly arranged and cannot compensate for the displaced amino group engaged in transition state stabilization, a finding that is in keeping with earlier results on a replacement of active site $Glu^{223}$ of LC/A with aspartate (*19*).

Mutation of amino acids delivering a hydrogen atom to the amide nitrogen would explicitly be expected to display serious detrimental effects on enzyme activity. Therefore, $Glu^{223}$ of the HisGluXXHis motif of BoNT/A, mutation of which generates enzymes with undetectable proteolytic activity except for a minimal residual activity for a conservative exchange to aspartate (*19*, *27*), presumably exercises a function corresponding to $Glu^{143}$ of thermolysin. This residue has been proposed to catalyze two consecutive proton transfers from the attacking $Zn^{2+}$-bound water molecule (*12*).

*Role of $Glu^{350}$ in Enzyme Activity.* The dramatic effect of mutating $Glu^{350}$ on enzyme activity (reduction of $k_{cat}$ by a factor of approximately $10^4$) is more difficult to reconcile. A mutation of the corresponding residues in thermolysin and the angiotensin I-converting enzyme to alanine decreases $k_{cat}$ by factors of only 4 and 9, respectively (*24*, *28*). Plausible explanations for this discrepancy arise from their crystal structures. In both of these gluzincins, an aspartate side chain is situated in place of $Glu^{350}$, which has been proposed in the case of thermolysin ($Asp^{226}$) to stay in hydrogen bonding interaction with the transition state stabilizing $His^{231}$ to keep its imidazole ring in a suitable position and to stabilize its charge during the transition state. Thus, this residue is likely not directly involved in the catalytic process. Hence, it is even more difficult to interpret the severe impact of mutating LC/A $Glu^{350}$, which radically exceeded the effects of replacing residues that are directly involved in catalysis; i.e., $Arg^{362}$ and $Tyr^{365}$ were replaced. $Glu^{350}$ is located in both LC/A and LC/B in the proximity of the transition state stabilizing $Arg^{362}$ ($Arg^{369}$ in LC/B) and $His^{222}$ ($His^{229}$ in LC/B), the latter one providing one of the four coordination sites for $Zn^{2+}$. On the other hand, $Asp^{226}$ of thermolysin does not interact with the imidazole ring of the corresponding $His^{146}$ as deduced from the crystal structure. From these data, it could be proposed that the major function of $Glu^{350}$ persists in stabilizing the structure of the active site by preserving the optimal positions of $Arg^{362}$ and $His^{222}$. This idea is supported by a reduced affinity for $Zn^{2+}$ and an increased sensitivity toward heat stress for mutants of $Glu^{350}$ (Table 3 and Figure 3). It appears that $Glu^{350}$ forms crucial ionic interactions, since LC/A($Glu^{350}$Gln), in which H-bond interactions with $His^{222}$ and $Arg^{362}$ still continue as predicted by molecular modeling, and LC/A($Glu^{350}$Ala) affected enzyme activity to a similar extent. An analogous role was recently assigned to the corresponding amino acid of neprilysin, $Asp^{709}$, mutation of which also diminished enzyme activity to a greater extent than mutation of the transition state stabilizing $His^{711}$ (*24*).

In conclusion, the clostridial neurotoxin gluzincin metalloprotease family (M27) holds, in addition to its unique substrate requirements, an unparalleled protein hydrolysis mechanism. Here, the side groups of a tyrosine and an arginine residue stabilize the transition state oxyanion, thus resembling members of the thermolysin family (family M4; *4*), in which two residues also assist this catalytic step. At variance, thermolysin family members engage a tyrosine and a histidine residue. On the other hand, this job is delegated to lone tyrosine or histidine residues in many other zinc-dependent metalloprotease families (*24*). $Glu^{350}$ (position in LC/A) of clostridial neurotoxins mainly possesses a crucial structural function that persists in optimal positioning of the oxyanion stabilizing arginine and of the proximal $Zn^{2+}$-coordinating histidine residue through ionic interactions.

## ACKNOWLEDGMENT

We thank Dr. G. Wünsch (University of Hannover, Hannover, Germany) for his help with the zinc content determinations, M. Enge, S. Feldhege, and T. Schaper for excellent technical assistance, and U. Matti for stimulating discussions.

## REFERENCES

1. Niemann, H., Blasi, J., and Jahn, R. (1994) *Trends Cell Biol. 4*, 179−185.
2. Schiavo, G., Matteoli, M., and Montecucco, C. (2000) *Physiol. Rev. 80*, 717−766.
3. Hooper, N. M. (1994) *FEBS Lett. 354*, 1−6.
4. Rawlings, N. D., and Barrett, A. J. (1995) *Methods Enzymol. 248*, 183−228.
5. Shone, C. C., Quinn, C. P., Wait, R., Hallis, B., Fooks, S. G., and Hambleton, P. (1993) *Eur. J. Biochem. 217*, 965−971.
6. Schiavo, G., Shone, C. C., Bennett, M., Scheller, R. H., and Montecucco, C. (1995) *J. Biol. Chem. 270*, 10566−10570.
7. Yamasaki, S., Baumeister, A., Binz, T., Blasi, J., Link, E., Cornille, F., Roques, B., Fykse, E. M., Südhof, T. C., Jahn, R., and Niemann, H. (1994) *J. Biol. Chem. 269*, 12764−12772.
8. Lacy, D. B., Tepp, W., Cohen, A. C., DasGupta, B. R., and Stevens, R. C. (1998) *Nat. Struct. Biol. 5*, 898−902.
9. Lacy, D. B., and Stevens, R. C. (1999) *J. Mol. Biol. 291*, 1091−1104.
10. Swaminathan, S., and Eswaramoorthy, S. (2000) *Nat. Struct. Biol. 7*, 693−699.
11. Yamasaki, S., Hu, Y., Binz, T., Kalkuhl, A., Kurazono, H., Tamura, T., Jahn, R., Kandel, E., and Niemann, H. (1994) *Proc. Natl. Acad. Sci. U.S.A. 91*, 4688−4692.
12. Hangauer, D. G., Monzingo, A. F., and Matthews, B. W. (1984) *Biochemistry 23*, 5730−5741.
13. Hanson, M. A., and Stevens, R. C. (2000) *Nat. Struct. Biol. 7*, 687−692.
14. Rossetto, O., Caccin, P., Rigoni, M., Tonello, F., Bortoletto, N., Stevens, R. C., and Montecucco, C. (2001) *Toxicon 39*, 1151−1159.
15. Binz, T., Blasi, J., Yamasaki, S., Baumeister, A., Link, E., Südhof, T. C., Jahn, R., and Niemann, H. (1994) *J. Biol. Chem. 269*, 1617−1620.
16. Vaidyanathan, V. V., Yoshino, K., Jahnz, M., Dörries, C., Bade, S., Nauenburg, S., Niemann, H., and Binz, T. (1999) *J. Neurochem. 72*, 327−337.
17. Guan, K. L., and Dixon, J. E. (1991) *Anal. Biochem. 192*, 262−267.
18. Sreerama, N., and Woody, R. W. (2000) *Anal. Biochem. 287*, 252−260.
19. Li, L., Binz, T., Niemann, H., and Singh, B. R. (2000) *Biochemistry 39*, 2399−2405.
20. Shone, C. C., and Roberts, A. K. (1994) *Eur. J. Biochem. 225*, 263−270.

21. Schiavo, G., and Montecucco, C. (1995) *Methods Enzymol. 248*, 643−652.
22. Mock, W. L., and Aksamawati, M. (1994) *Biochem. J. 302*, 57−68.
23. Beaumont, A., O'Donohue, M. J., Paredes, N., Rousselet, N., Assicot, M., Bohuon, C., Fournie-Zaluski, M.-C., and Roques, B. P. (1995) *J. Biol. Chem. 270*, 16803−16808.
24. Marie-Claire, C., Ruffet, E., Tiraboschi, G., and Fournie-Zaluski, M.-C. (1998) *FEBS Lett. 438*, 215−219.
25. Fersht, A. R., Shi, J.-P., Knill-Jones, J., Lowe, D. M., Wilkinson, A. J., Blow, D. M., Brick, P., Carter, P., Waye, M. M. Y., and Winter, G. (1985) *Nature 314*, 235−238.
26. Dion, N., Le Moual, H., Crine, P., and Boileau, G. (1993) *FEBS Lett. 318*, 301−304.
27. Blasi, J., Chapman, E. R., Link, E., Binz, T., Yamasaki, S., DeCamilli, P., Südhof, T. C., Niemann, H., and Jahn, R. (1993) *Nature 365*, 160−163.
28. Fernandez, M., Liu, X., Wouters, M. A., Heyberger, S., and Husain, A. (2001) *J. Biol. Chem. 276*, 4998−5004.
29. Schechter, I., and Berger, A. (1967) *Biochem. Biophys. Res. Commun. 27*, 157−162.

BI0157969